SILICON X-RAY LINE EMISSION FROM SOLAR FLARES AND ACTIVE REGIONS

JOHN H. PARKINSON

Columbia Astrophysics Laboratory, Columbia University
and
Mullard Space Science Laboratory, University College London, Holmbury St. Mary, Dorking, Surrey, England

and

R. S. WOLFF*, H. L. KESTENBAUM**, W. H.-M. KU, J. R. LEMEN, K. S. LONG, R. NOVICK, R. J. SUOZZO, and M. C. WEISSKOPF§

Columbia Astrophysics Laboratory, Departments of Astronomy and Physics, Columbia University, New York, N.Y. 10027, U.S.A.

(Received 18 April; in revised form 4 August, 1978)

Abstract. New observations of solar flare and active region X-ray spectra obtained with the Columbia University instrument on OSO-8 are presented and discussed. The high sensitivity of the graphite crystal panel has allowed both line and continuum spectra to be observed with moderate spectral resolution. Observations with higher spectral resolution have been made with a panel of pentaerythritol crystals. Twenty-nine lines between 1.5 and 7.0 Å have been resolved and identified, including several dielectronic recombination satellite lines to Si XIV and Si XIII lines which have been observed for the first time. It has been found that thermal continuum models specified by single values of temperature and emission measure have fitted the data adequately, there being good agreement with the values of these parameters derived from line intensity ratios.

1. Introduction

The solar corona allows us to take a unique glimpse at high temperature ($\gtrsim 10^6$ K), low density ($\lesssim 10^{15}$ cm^{-3}) plasma. In the X-ray region the line emission spectrum is characteristic of highly stripped ions and is rich in multiplet structure. By observing the corona under a variety of conditions, many of the observed lines have been identified and much has been learned about the physical processes that give rise to the observed transitions.

Over the past few years several instruments have been flown on satellites which have contributed greatly to our understanding of the solar flare X-ray spectrum, and thereby the conditions in the corona (e.g., Walker, 1972; Doschek, 1972; Švestka, 1976, and references therein). These instruments have been limited either by poor spectral resolution or by low sensitivity, giving little or no information on the spectral

* Present address: Bell Telephone Laboratories, Inc., Crawford Hill Laboratory, P.O. Box 400, Holmdel, N.J. 07733. U.S.A.

** Present address: Anistics Division of Alexander & Alexander, Inc., 640 Fifth Avenue, New York, N.Y. 10019, U.S.A.

§ Present address: Code ES-62, NASA George C. Marshall Space Flight Center, Marshall Space Flight Center, Ala. 35812, U.S.A.

Solar Physics **60** (1978) 123–136.

development of dynamic events. Most have been poorly calibrated making a quantitative investigation difficult.

In this paper we report on observations made with the Columbia University Bragg crystal spectrometers on board the Orbiting Solar Observatory, OSO-8, satellite, which attempt to overcome some of these limitations which have compromised earlier instruments. High sensitivity and good time resolution are obtained by using a large panel of coaligned graphite crystals which are highly reflective to X-rays. Good spectral resolution is achieved with a smaller panel of pentaerythritol (PET) crystals. These spectrometers have enabled us to obtain solar spectra under quiescent and flare conditions. Here we present examples of such spectra, concentrate on the analysis of the Si XII, Si XIII, and Si XIV lines, and investigate the usefulness of such lines for deriving the physical conditions in the emitting plasma. Several lines are observed for the first time, and their identifications and intensities are discussed.

2. Instrumentation

The Columbia University solar instrument on the OSO-8 satellite has been obtaining X-ray spectra of the Sun during the daylight portion of each orbit since launch in June 1975. The instrument consists of two spectrometers, one employing a panel of coaligned graphite crystals to obtain high sensitivity, moderate resolution spectra, and the other a panel of coaligned PET crystals which have higher spectral resolution but a lower sensitivity. Key parameters are summarized in Table I, and more details are given by Wolff (1976) and Kestenbaum *et al.* (1976).

TABLE I

Key parameters of the graphite and PET spectrometers

Parameter	Graphite	PET
$2d$ (d = crystal interplanar spacing) (Å)	6.67	8.726
Rocking curve width (degrees)	0.8	0.10
Wavelength range (Å)	1.5–6.7	5.13–7.18
Angular bin size (degrees)	0.163	0.038
Geometrical area per resolution element (cm^2)	100	3
Typical response for line emission (counts per revolution detected for incident flux of 1 erg $(cm^2\ s)^{-1}$)	3×10^7	1×10^5

The instrument is located in the wheel section of the satellite and views the Sun once a revolution (nominally 10 s) along a radial direction. The crystals are fixed relative to the wheel, and a full Bragg angle scan is thus achieved by the wheel rotation. The reflected photons are detected in a fixed bank of proportional counters, and the data are accumulated into 512 time bins (proportional to Bragg angle).

Other satellite-borne X-ray spectrometers working in the 1.5–7.0 Å range have employed scanning crystals and have had considerably worse time resolution, thus

compromising their usefulness when observing rapidly varying phenomena. For example, the average time resolution of the Aerospace instrument on OV1-17 was 24 min (Walker and Rugge, 1970), for the NRL instrument on OSO-6 it was 8 min (Doschek *et al.*, 1971), and for the Goddard instrument on OSO-5 it was 2.5 min (Neupert, 1971). Combined with the high sensitivity of the graphite crystals, the good time resolution of the Columbia University instrument has allowed several rapidly varying phenomena to be observed for the first time. Effects such as possible density changes indicated by the S XV lines and satellite line intensity variations with temperature will be dealt with in subsequent papers.

The spectrometers are uncollimated and view the whole Sun on each rotation. Thus the problem of overlapping spectra arises due to a range of angles of incidence being presented simultaneously when more than one active region is present on the solar disk (Parkinson, 1976). Flare observations are not affected as around the time of solar minimum there has generally been sporadic activity so the probability of having flares in two active regions simultaneously has been low.

3. Observations with the Graphite Spectrometer

The graphite spectrometer has been calibrated both in the laboratory and with nonsolar X-ray sources, and the uncertainty in the instrument response function is believed to be less than ±10% (Kestenbaum *et al.*, 1976).

Two typical spectra of different levels of solar activity are shown in Figures 1 and 2. The first spectrum shows an average obtained between 08:41 and 08:58 UT around the peak of a subflare on 18 November 1975. The second was obtained between 09:08 and 09:25 UT immediately after this burst and represents the convolved spectrum of two active regions that were present on the solar disk. These two figures demonstrate clearly how the strong line and continuum radiations vary with the level of solar activity. They also demonstrate the advantage of using a highly reflective crystal such as graphite in that the thermal continuum is always observed even from nonflaring active regions.

3.1. The continuum

The thermal continuum has been estimated from the observed spectra by fitting to 104 bins, spread throughout the spectrum and carefully chosen so as to be free from line emission. The expression used is the simplified empirical expression of Culhane and Acton (1970) which they showed was always within 15% of the full expression derived by Culhane (1969) for the wavelength and temperature ranges discussed in the present paper.

The best fits to the continua in Figures 1 and 2 are shown on these figures. The corresponding temperatures and emission measures are given in the figure captions and will be discussed later. Note that here the continua have been folded through the instrument response function which accounts for the uneven nature of the curve. At first sight, it is remarkable that a continuum specified by a single temperature is such a

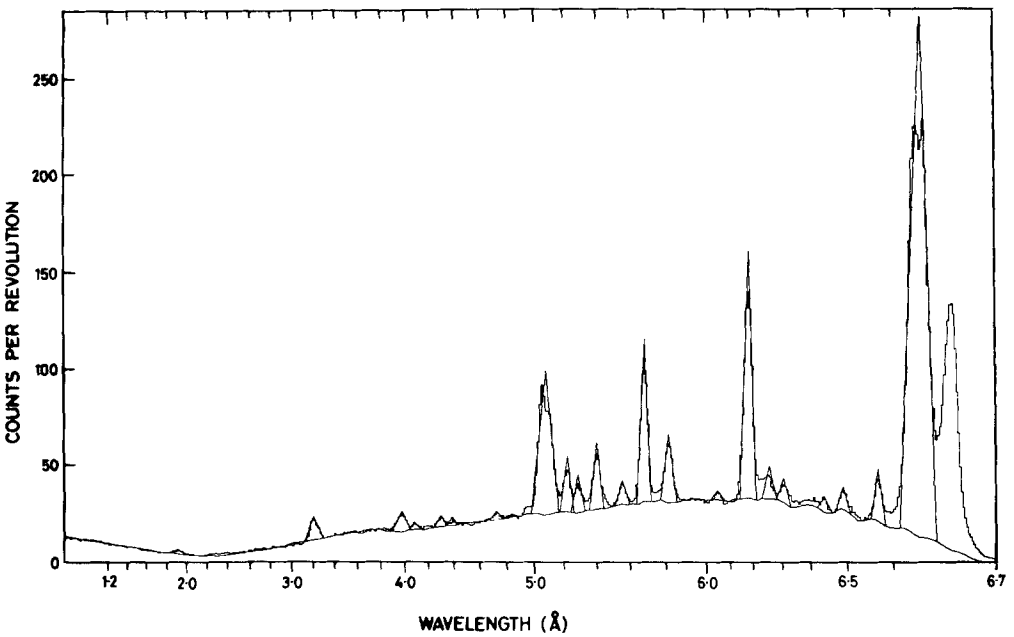

Fig. 1. An X-ray spectrum obtained with the graphite crystal spectrometer during a subflare, 08:41–08:58 UT, 18 November 1975. The best-fitting continuum and line profiles, derived as described in the text, are shown. The continuum temperature represented is 8.2×10^{6} K, and the emission measure is 1.2×10^{48} cm^{-3}

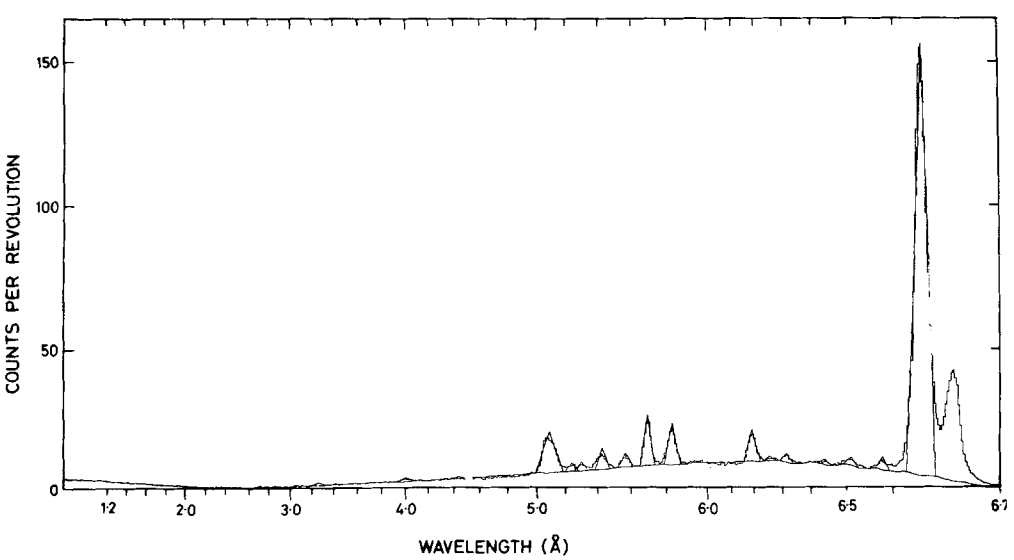

Fig. 2. An active region X-ray spectrum obtained with the graphite crystal spectrometer between 09:08 and 09:25 UT, 18 November 1975, shortly after the subflare shown in Figure 1. The continuum temperature is 5.6×10^{6} K, and the emission measure is 8.6×10^{47} cm^{-3}

good fit to the data, when one considers that previous authors have found poor fits for single temperature models, e.g., Herring and Craig (1973). Most previous attempts at fitting continuum models in this spectral range have been made with data from proportional counters with only a few pulse height channels and have thus been unable to resolve the lines from the continuum. It is likely that these previous attempts have been hampered by this problem and by the omission of important strong lines.

3.2. The lines

An attempt has been made to compute automatically the intensities of all the lines present in any graphite spectrum. The procedure adopted first subtracts the calculated thermal continuum from the data and finds the best-fitting profile for each line. A triangular profile is used in Figures 1 and 2 and appears to fit well for single lines with FWHM between 0.5° and 0.7°, except for the Si XIII helium-like resonance line at 6.64 Å. The routine first finds the centroid of the excess emission and for a predetermined width determines the best-fitting peak value as judged by the value of the χ^2 parameter. Where lines are blended, the blend is generally observed to have a more rectangular profile, and this method fits preferentially to the sides of the profile, so overestimating the peak value.

Table II lists the wavelengths and intensities of the lines shown in Figures 1 and 2 together with the proposed identifications. For line blends the most appropriate description is given. For each of the helium-like ions between S and Ca, the resonance, intercombination, and forbidden lines are all blended together with many satellite lines. The line at 1.91 Å is identified as a blend of several dielectronic recombination satellite and inner shell lines in Fe XVII–XXV, and will be discussed in a later publication. Several satellite lines to the $1s-np$, Lyman series and to the $1s^2-1s\ np$ series are identified, some for the first time. As can be seen from the observations already presented, these often approach the strength of the principal lines to which they are satellites.

4. Observations with the PET Spectrometer

As mentioned earlier, the PET spectrometer has a considerably greater spectral resolving power than the graphite spectrometer, which, combined with the lower sensitivity, makes it very useful for observing large flares. Figure 3 shows data obtained with this spectrometer between 19:45 and 19:56 UT on 18 November 1975 during another subflare in the same active region as the event discussed earlier.

A line profile fitting program, similar to that used to analyze the graphite spectrometer data, has been used to derive the intensities of the observed lines, and these are listed in Table III. The calibration of the PET spectrometer is based only on laboratory tests and may be uncertain by as much as 30%. Almost half of the lines are identified as satellite lines, and these identifications are discussed in later sections.

TABLE II

Wavelengths, intensities, and proposed identifications of lines observed with the graphite spectrometer on 18 November 1975

Wavelength (Å)	Line intensity (erg (cm^2 s)$^{-1}$)		Identification		
	08:41–08:58 UT	09:08–09:25 UT	Ion	Lower level	Upper level
1.913	4.8×10^{-7}		Fe XVII-XXV		See text
3.209	2.0×10^{-6}	1.7×10^{-7}	Ca XIX		Helium-like
3.981	2.3×10^{-6}	2.8×10^{-7}	Ar XVII		Helium-like
4.087	5.6×10^{-7}				
4.302	8.3×10^{-7}		S XV	$1s^2\,.\,{}^1S_0$	$1s\,3p\,.\,{}^1P_1$
4.390	6.3×10^{-7}		S XIV	$1s^2\,.\,nl$	$1s\,3p\,.\,nl$
4.729	5.4×10^{-7}		S XVI	$1s\,.\,{}^2S_{1/2}$	$2p\,.\,{}^2P_{1/2,3/2}$
4.842	2.2×10^{-7}		Si XIV	$1s\,.\,{}^2S_{1/2}$	$5p\,.\,{}^2P_{1/2,3/2}$
5.071	2.0×10^{-5}	4.0×10^{-6}	S XV		Helium-like
5.217	3.8×10^{-6}	4.1×10^{-7}	Si XIV	$1s\,.\,{}^2S_{1/2}$	$3p\,.\,{}^2P_{1/2,3/2}$
5.288	2.7×10^{-6}	4.4×10^{-7}	Si XIII	$1s^2\,.\,{}^1S_0$	$1s\,5p\,.\,{}^1P_1$
5.405	4.4×10^{-6}	9.5×10^{-7}	Si XIII	$1s^2\,.\,{}^1S_0$	$1s\,4p\,.\,{}^1P_1$
5.558	1.3×10^{-6}	5.5×10^{-7}	Si XII	$1s^2\,.\,\binom{2p}{2s}$	$1s\,4p\,.\,\binom{2p}{2s}$
5.680	8.7×10^{-6}	1.9×10^{-6}	Si XIII	$1s^2\,.\,1S_0$	$1s\,3p\,.\,{}^1P_1$
5.811	4.0×10^{-6}	1.7×10^{-6}	Si XII	$1s^2\,.\,\binom{2p}{2s}$	$1s\,3p\,.\,\binom{2p}{2s}$
6.049	4.2×10^{-7}		Al XIII	$1s\,.\,{}^2S_{1/2}$	$3p\,.\,{}^2P_{1/2,3/2}$
6.178	1.1×10^{-5}	9.9×10^{-7}	Si XIV	$1s\,.\,{}^2S_{1/2}$	$2p\,.\,{}^2P_{1/2,3/2}$
6.260	1.3×10^{-6}	1.2×10^{-7}	Si XIII	$1s\,.\,\binom{2p}{2s}$	$2p\,.\,\binom{2p}{2s}$
6.311	9.3×10^{-7}	2.3×10^{-7}	Al XII	$1s^2\,.\,{}^1S_0$	$1s\,4p\,.\,{}^1P_1$
6.441	6.0×10^{-7}	1.5×10^{-7}	Mg XII	$1s\,.\,{}^2S_{1/2}$	$7p\,.\,{}^2P_{1/2,3/2}$
6.492	7.7×10^{-7}	2.0×10^{-7}	Mg XII	$1s\,.\,{}^2S_{1/2}$	$6p\,.\,{}^2P_{1/2,3/2}$
6.572	1.8×10^{-6}	3.1×10^{-7}	Mg XII	$1s\,.\,{}^2S_{1/2}$	$5p\,.\,{}^2P_{1/2,3/2}$
6.641	5.0×10^{-5}	2.3×10^{-5}	Si XIII	$1s^2\,.\,{}^1S_0$	$1s\,2p\,.\,{}^1P_1$

After the position of the flaring region on the Sun has been taken into account, the measured wavelengths are seen to be in excellent agreement with previous solar and laboratory values. The strong lines agree to better than ±0.002 Å and the weak lines to better than ±0.004 Å.

5. Observations of Si XIV and Related Satellite Lines

The Lyman series of Si is always prominent in spectra obtained during bursts, as shown in Figure 1, and we have often used the intensity of the Lα line as an index for assessing the level of solar activity. Note that the Lγ line is omitted from Table II. It appears at 4.95 Å and is blended with the wing of the S XV complex.

In Figures 1 and 2 it is clear that there is a satellite line of the type $1s\,.\,nl-2p\,.\,nl$, just on the long wavelength side of the Lα line, at 6.26 Å. With the PET spec-

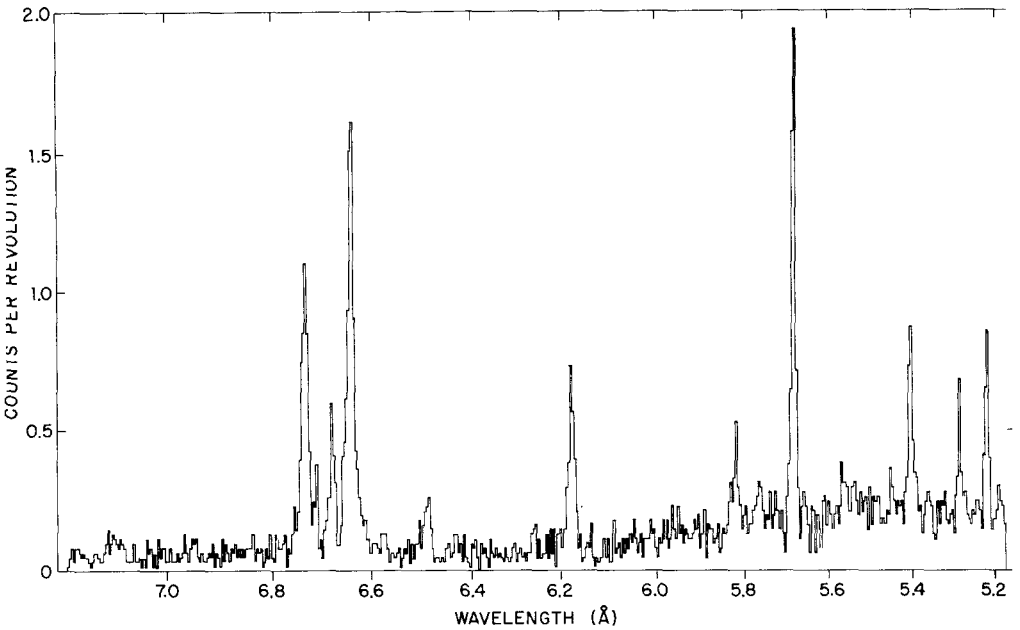

Fig. 3. A subflare spectrum obtained with the PET spectrometer between 19:45 and 19:56 UT on 18 November 1975.

TABLE III

Wavelengths, intensities, and proposed identifications of lines observed with the PET spectrometer on 18 November 1975 at 19:45–19:56 UT

Wavelength (Å)	Line intensity (erg (cm^2 s)$^{-1}$)	Identification		
		Ion	Lower level	Upper level
5.217	1.6×10^{-5}	Si XIV	$1s\,.\,^2S_{1/2}$	$3p\,.\,^2P_{1/2,3/2}$
5.285	7.6×10^{-6}	Si XIII	$1s^2\,.\,^1S_0$	$1s\,5p\,.\,^1P_1$
5.404	1.5×10^{-5}	Si XIII	$1s^2\,.\,^1S_0$	$1s\,4p\,.\,^1P_1$
5.450	4.5×10^{-6}	Si XII	$1s^2\,.\,2p\,.\,^2P$	$1s\,5p\,.\,2p\,.\,^2D$
5.487	3.8×10^{-6}	Si XII	$1s^2\,.\,2s\,.\,^2S$	$1s\,4p\,.\,2s\,.\,^2P$
5.565	7.0×10^{-6}	Si XII	$1s^2\,.\,2p\,.\,^2P$	$1s\,4p\,.\,2p\,.\,^2D$
5.681	3.1×10^{-5}	Si XIII	$1s^2\,.\,^1S_0$	$1s\,3p\,.\,^1P_1$
5.762	5.1×10^{-6}	Si XII	$1s^2\,.\,2s\,.\,^2S$	$1s\,3p\,.\,2s\,.\,^2P$
5.818	9.6×10^{-6}	Si XII	$1s^2\,.\,2p\,.\,^2P$	$1s\,3P\,.\,2p\,.\,^2D$
6.184	2.1×10^{-5}	Si XIV	$1s\,.\,^2S_{1/2}$	$2p\,.\,^2P_{1/2,3/2}$
6.268	3.6×10^{-6}	Si XIII	$1s\,2p\,.\,^1P_1$	$2p^2\,.\,^1D_2$
6.492	8.2×10^{-6}	Mg XII	$1s\,.\,^2S_{1/2}$	$6p\,.\,^2P_{1/2,3/2}$
6.646	4.7×10^{-5}	Si XIII	$1s^2\,.\,^1S_0$	$1s\,2p\,.\,^1P_1$
6.685	1.4×10^{-5}	Si XIII	$1s^2\,.\,^1S_0$	$1s\,2p\,.\,^3P_1$
6.717	6.3×10^{-6}	Si XII	$1s^2\,.\,2s\,.\,^2S$	$1s\,2p\,.\,2s\,.\,^2P$
6.738	3.4×10^{-5}	Si XIII	$1s^2\,.\,^1S_0$	$1s\,2s\,.\,^3S_1$

trometer the strongest line is observed at 6.268 Å with several lines of lower significance closer to the Lα line, as shown in Figure 4.

Meekins *et al.* (1970) were the first to observe such a line at 6.265 Å but were unable to identify it. Neupert (1971) observed a line at 6.246 Å which he claimed was a satellite line but was unable to be specific. We are now able to identify the line we observe at 6.268 Å as $1s\,2p\,.\,{}^1P_1 - 2p^2\,.\,{}^1D_2$ in Si XIII. This is confirmed by both Feldman *et al.* (1974) and Boiko *et al.* (1977) who have observed laser-produced plasmas and found the above transition gave the strongest satellite line in their spectra, which was observed at 6.263 Å and 6.264 Å, respectively.

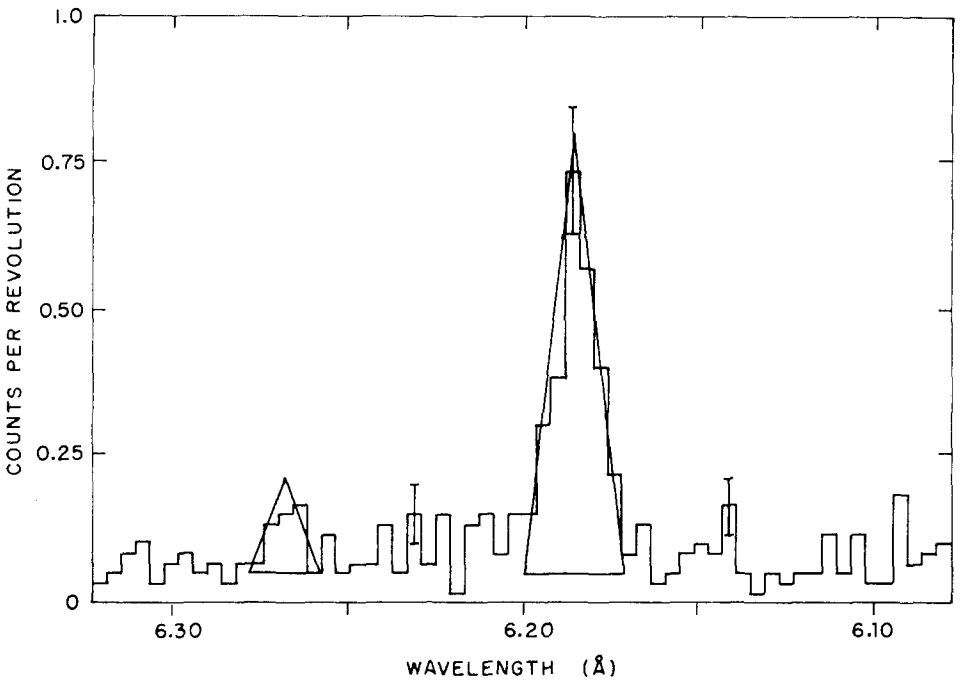

Fig. 4. A portion of the PET spectrum of Figure 3. The lines shown as the Si XIV Lα line (6.18 Å) and the $1s\,2p\,.\,{}^1P_1 - 2p^2\,.\,{}^1D_2$ satellite line in Si XIII (6.27 Å). The vertical error bars are $\pm 1\sigma$ and represent the statistical uncertainty on the instantaneous counting rate.

6. Observations of Si XIII and Related Satellite Lines

An enlargement of the region between 6.6 and 6.8 Å observed with the PET spectrometer is shown in Figure 5. The helium-like resonance $1s^2\,.\,{}^1S_0 - 1s\,2p\,.\,{}^1P_1$, intercombination $1s^2\,.\,{}^1S_0 - 1s\,2p\,.\,{}^3P_1$, and forbidden $1s^2\,.\,{}^1S_0 - 1s\,2s\,.\,{}^3S_1$ lines in Si XIII are clearly resolved together with the $1s^2\,.\,2s\,.\,{}^2S - 1s\,2p\,.\,2s\,.\,{}^2P$ satellite line (Gabriel and Jordan, 1972; Gabriel, 1972).

In Figure 5 it appears that a triangle is an oversimplification of the observed line profile which is likely to be closer to a Lorentzian distribution. However, it is noticeable that the resonance line is somewhat asymmetric with excess emission on

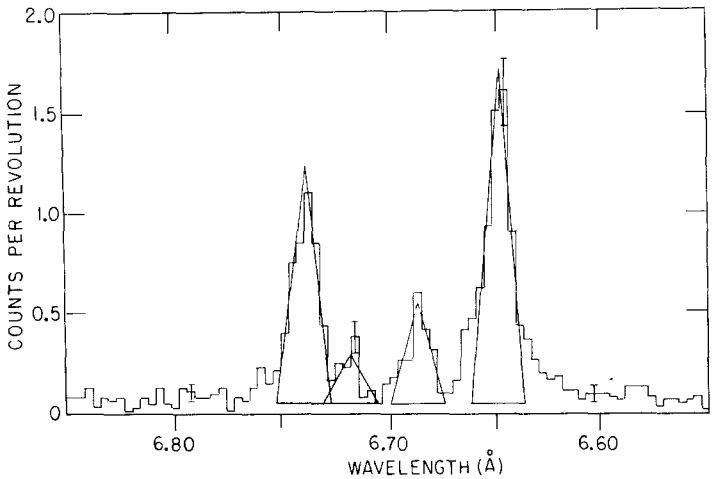

Fig. 5. The resonance $1s^2\,.\,{}^1S_0-1s\,2p\,.\,{}^1P_1$ (6.65 Å), intercombination $1s^2\,.\,{}^1S_0-1s\,2p\,.\,{}^3P_1$ (6.69 Å), and forbidden $1s^2\,.\,{}^2S_0-1s\,2s\,.\,{}^3S_1$ (6.74 Å) lines of Si XIII, together with the $1s^2\,.\,2s\,.\,{}^2S-1s\,2p\,.\,2s\,.\,{}^2P$ (6.72 Å) satellite line, observed with the PET spectrometer.

the long wavelength side. This is due to unresolved satellite lines of the type $1s^2\,.\,ml-1s\,2p\,.\,ml$, $m\geq 3$, which have also been observed in Mg and Ne (Parkinson, 1971, 1972). There appears to be an excess on the long wavelength side of the forbidden line around 6.76 Å. If this feature is real, then its origin is unknown, as it cannot be due to the $1s^2\,.\,2s\,.\,2S-1s\,2p\,.\,2s\,.\,{}^4P$ satellite lines which can only be excited by inner shell processes and are predicted to lie in the range 6.78–6.79 Å by Gabriel (1972).

The major features in Figures 1 and 2 that have not previously been discussed in detail elsewhere are the satellite lines to the $1s^2-1s\,3p$ and $1s^2-1s\,4p$ lines in Si XII, observed at 5.81 Å and 5.56 Å. The graphite spectrometer data show the satellite: principal line flux ratio decreases strongly with increasing solar activity (i.e., temperature) as shown in Table IV. In Section 7.3 we will show that the upper levels

TABLE IV

Satellite: principal line ratios

Line ratio	Flare spectrum (Fig. 1)	Active region spectrum (Fig. 2)
$\dfrac{I\left[1s^2\,.\,\binom{2p}{2s}-1s\,3p\,.\,\binom{2p}{2s}\right]}{I[1s^2-1s\,3p]}$	0.46	0.89
$\dfrac{I\left[1s^2\,.\,\binom{2p}{2s}-1s\,4p\,.\,\binom{2p}{2s}\right]}{I[1s^2-1s\,4p]}$	0.30	0.58

of such satellite lines are formed principally by the dielectronic recombination process.

Most of the previous spectrometers operating in the 5–6 Å wavelength range have only been sensitive to large X-ray bursts, which is when the relative intensity of these satellite lines is lowest, and so they may often have gone undetected. The line at 5.81 Å was first noted by Meekins *et al.* (1970) who did not propose an identification. From a later observation, Walker and Rugge (1971) proposed that this line was a blend of the $1s^2 . 2s . {}^2S - 1s\ 3p . 2s . {}^2P$ line at 5.797 Å and the $1s^2 . 2p . {}^2P - 1s\ 3p . 2p . {}^2D$ line at 5.817 Å.

When the higher resolution PET observations are used, the 5.81 Å line does split into at least two components as shown in Figure 6. These lines are observed at 5.818 Å (15 standard deviations above the background) and 5.762 Å (8σ) in the solar spectrum, and they are also observed to be the strongest lines in the spectrum of the laser-produced plasma of Feldman *et al.* (1974), who give wavelengths of 5.816 and 5.768 Å.

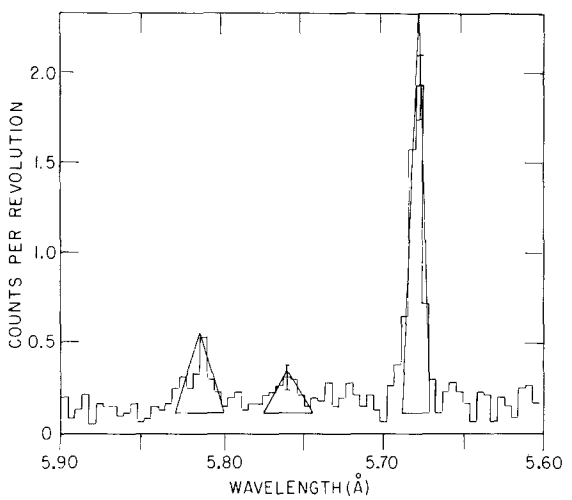

Fig. 6. The $1s^2 . {}^1S_0 - 1s\ 3p . {}^1P_1$ (5.68 Å) line of Si XIII, together with the $1s^2 . 2s . {}^2S - 1s\ 3p . 2s . {}^2P$ (5.76 Å) and $1s^2 . 2p . {}^2P - 1s\ 3p . 2p . {}^2D$ (5.82 Å) satellite lines.

The line at 5.56 Å does not appear to have been reported previously, but as it is observed to have a temperature dependence which is very similar to that for the line at 5.81 Å, it must basically be due to satellite lines of the type $1s^2 . 2l - 1s\ 4p . 2l$. With the PET spectrometer this line is resolved into at least three components as shown in Figure 7. None of the satellite line fits are entirely satisfactory, and this may be due to line blending or to the inherent weakness of the lines.

Having identified the lines at 5.82 and 5.76 Å as $1s^2 . 2p . {}^2P - 1s\ np . 2p . {}^2D$ and $1s^2 . 2s . {}^2S - 1s\ np . 2s . {}^2P$ with $n = 3$, we are then able to extrapolate along the above series to $n = 4$ and 5. Such a procedure enables the lines at 5.565 Å (7σ) and

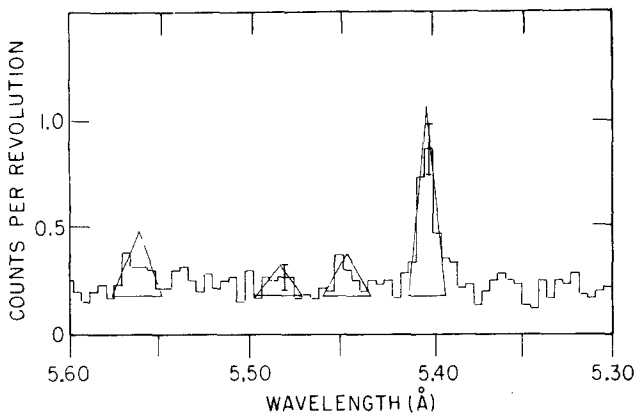

Fig. 7. The $1s^2\,.\,{}^1S_0 - 1s\,4p\,.\,{}^1P_1$ (5.40 Å) line of Si XIII, together with the $1s^2\,.\,2p\,.\,{}^2P - 1s\,5p\,.\,2p\,.\,{}^2D$ (5.45 Å), $1s^2\,.\,2s\,.\,{}^2S - 1s\,4p\,.\,2s\,.\,{}^2P$ (5.49 Å), and $1s^2\,.\,2p\,.\,{}^2P - 1s\,4p\,.\,2p\,.\,{}^2D$ (5.57 Å) satellite lines.

5.487 Å (3σ) to be identified as these respective transitions with $n = 4$, and the line at 5.450 Å (4σ) is identified with $n = 5$ and a $2p$ shielding electron. The corresponding line for $n = 5$ and a $2s$ shielding electron is predicted to lie at 5.364 Å, where a weak, barely significant feature, not included in Table III but visible in Figure 7, is observed.

7. Discussion

7.1. Comparison of the temperatures for the continuum and the Si lines

In Section 3 we discussed how a characteristic temperature and emission measure could be determined from the observed continuum. It is also possible to estimate such parameters from line ratios; see, for example, Parkinson (1975). A particularly useful pair of lines is Si XIII and Si XIV, as the temperature derived is independent of the abundance of Si. Table V lists the temperatures and emission measures for these

TABLE V

Comparison of temperatures (T_e) and emission measures ($N_e^2 V$) derived from the Si lines and the continuum

	Flare spectrum (Fig. 1)	Active region spectrum (Fig. 2)
Si XIII : Si XIV		
T_e (K)	8.7×10^6	6.3×10^6
$N_e^2 V$ (cm^{-3})	5.3×10^{47}	3.8×10^{47}
Continuum		
T_e (K)	8.2×10^6	5.6×10^6
$N_e^2 V$ (cm^{-3})	1.2×10^{48}	8.6×10^{47}

lines, derived by using the ionization balance calculations of Jordan (1969), and compares these with the values obtained from the continuum. The temperature derived from the lines is approximately 0.5×10^6 K greater than that from the continuum, and the emission measure is approximately half that for the continuum. The line intensities that would be predicted from the continuum temperature and emission measure are always within ±50% of the observed values, so the differences mentioned above are not significant.

7.2. The Si XIII helium-like lines

Helium-like line systems have attracted much attention in the last few years because of the possibility of using the ratio of the forbidden line $1s^2\,.\,{}^1S_0-1s\,2s\,.\,{}^3S_1$: intercombination line $1s^2\,.\,{}^1S_0-1s\,2p\,.\,{}^3P_1$ to diagnose densities in coronal plasmas (Gabriel and Jordan, 1972, and references therein). For low densities the upper levels of these transitions are populated directly from, and decay to, the ground state. However, for sufficiently high densities collisional interchange from the $1s\,2s\,.\,{}^3S$ level to the $1s\,2p\,.\,{}^3P$ levels takes place. Using the nomenclature of Gabriel and Jordan, we find the above ratio R for the PET spectrum in Figure 5 is given by

$$R=\frac{I(1s^2\,.\,{}^1S_0-1s\,2s\,.\,{}^3S_1)}{I(1s^2\,.\,{}^1S_0-1s\,2p\,.\,{}^3P)}=2.4\pm0.3\,,$$

which should be compared with the low density limit for Si XIII of 2.2, corresponding to a density of 5.4×10^{12} cm^{-3} with F taken as 0.35 for a temperature of 6×10^6 K (Blumenthal *et al.*, 1972; Gabriel and Jordan, 1973).

The ratio G is given by

$$G=\frac{I(1s^2\,.\,{}^1S_0-1s\,2s\,.\,{}^3S_1)+I(1s^2\,.\,{}^1S_0-1s\,2p\,.\,{}^3P)}{I(1s^2\,.\,{}^1S_0-1s\,2p\,.\,{}^1P_1)}=1.0\pm0.1\,,$$

which is in agreement with the value of unity predicted by Gabriel and Jordan (1972) but higher than the value 0.7 predicted by Mewe and Schrijver (1978). However, the values of the ratios R and G will be affected by the presence of satellite lines. The $1s^2\,.\,2p\,.\,{}^2P-1s\,2p^2\,.\,{}^2D$ dielectronic recombination line in Si XII is predicted to be the strongest satellite line in this part of the spectrum, and is blended with the forbidden line (Bhalla *et al.*, 1975), making it difficult to look for differences from the low density limit. It is not possible to estimate the intensity of the $^2P-{}^2D$ line from the intensity of the $1s^2\,.\,2s\,.\,{}^2S-1s\,2p\,.\,2s\,.\,{}^2P$ line, which is observed at 6.72 Å, as the latter line has contributions from both dielectronic recombination and direct inner shell excitation.

7.3. The $1s^2\,.\,\binom{2p}{2s}-1s\,np\,.\,\binom{2p}{2s}$ line series

In Section 6 we discussed the identification of lines in these satellite line series. From Table IV, for $n=3$ and $n=4$, the ratio of satellite line: principal line increases by a factor of 1.93 from the flare spectrum to that of the active region. This behavior is

consistent with the purely dielectronic recombination temperature dependence for the $n = 2$ transitions given by Bhalla *et al.* (1975), who predict factors of 1.7 (using the line temperatures) and 1.9 (using the continuum temperatures) for this increase. The increase due to pure inner shell effects would only be a factor of 1.1.

From the higher resolution PET spectra, it is clear that for $n = 3$, 4, and 5, the line formed with a $2p$ spectator electron is always approximately twice the strength of the same line but with a $2s$ spectator.

8. Conclusions

In this paper we have presented typical graphite and PET spectra obtained with the Columbia University instrument on OSO-8. Twenty-nine lines have been resolved and identified between 1.5 and 7.0 Å. Fits have been made to the thermal continuum observed with the graphite spectrometer and compared with the temperature derived from the Si XIII and Si XIV lines. The line ratio gives a temperature approximately 0.5×10^6 K greater than that for the continuum and an emission measure approximately half that derived from the continuum. This is not a real discrepancy as the differences are compensatory. It is always possible to force the intensities of adjacent ions of the same element to give a single temperature, but it is remarkable that a single temperature continuum fits so well.

Members of the $1s^2 . 2s . {}^2S - 1s\,np . 2s . {}^2P$ and $1s^2 . 2p . {}^2P - 1s\,np . 2p . {}^2D$ series have been classified, for the first time, by extrapolating along these series from $n = 2$, 3 to $n = 4$, 5. For $n = 2$, there is a possibility that both dielectronic recombination and direct collisional excitation contribute to the line intensity, whereas the intensities of the satellite lines for $n = 3$ and 4 are consistent with their being formed purely by dielectronic recombination. The detailed study of these lines in flares will reveal their temperature dependence.

Acknowledgement

This work was supported by the National Aeronautics and Space Administration under contract NAS5-22408. This paper is Columbia Astrophysics Laboratory Contribution No. 137.

References

Bhalla, C. P., Gabriel, A. H., and Presnyakov, L. P.: 1975, *Monthly Notices Roy. Astron. Soc.* **172**, 359.
Blumenthal, G. R., Drake, G. W. F., and Tucker, W. H.: 1972, *Astrophys. J.* **172**, 205.
Boiko, V. A., Faenov, A. Y., Pikuz, S. A., and Safronova, U. I.: 1977, *Monthly Notices Roy. Astron. Soc.* **181**, 107.
Culhane, J. L.: 1969, *Monthly Notices Roy. Astron. Soc.* **144**, 375.
Culhane, J. L. and Acton, L. W.: 1970, *Monthly Notices Roy. Astron. Soc.* **151**, 141.
Doschek, G. A.: 1972, *Space Sci. Rev.* **13**, 765.
Doschek, G. A., Meekins, J. F., Kreplin, R. W., Chubb, T. A., and Friedman, H.: 1971, *Astrophys. J.* **164**, 165.

Feldman, U., Doschek, G. A., Nagel, D. J., Cowan, R. D., and Whitlock, R. R.: 1974, *Astrophys. J.* **192**, 213.
Gabriel, A. H.: 1972, *Monthly Notices Roy. Astron. Soc.* **160**, 99.
Gabriel, A. H. and Jordan, C.: 1972, in E. W. McDaniel and M. R. C. McDowell (eds.), *Case Studies in Atomic Collision Physics*, North-Holland, Amsterdam, Netherlands, Vol. 2, pp. 209–291.
Gabriel, A. H. and Jordan, C.: 1973, *Astrophys. J.* **186**, 327.
Herring, J. R. H. and Craig, I. J. D.: 1973, *Solar Phys.* **28**, 169.
Jordan, C.: 1969, *Monthly Notices Roy. Astron. Soc.* **142**, 501.
Kestenbaum, H. L., Cohen, G. G., Long, K. S., Novick, R., Silver, E. H., Weisskopf, M. C., and Wolff, R. S.: 1976, *Astrophys. J.* **210**, 805.
Meekins, J. F., Doschek, G. A., Friedman, H., Chubb, T. A., and Kreplin, R. W.: 1970, *Solar Phys.* **13**, 198.
Mewe, R. and Schrijver, J.: 1978, *Astron. Astrophys.* **65**, 99.
Neupert, W. M.: 1971, *Solar Phys.* **18**, 474.
Parkinson, J. H.: 1971, *Nature Phys. Sci.* **233**, 44.
Parkinson, J. H.: 1972, *Nature Phys. Sci.* **236**, 68.
Parkinson, J. H.: 1975, in S. R. Kane (ed.), 'Solar Gamma-, X-, and EUV Radiation', *IAU Symp.* **68**, 45.
Parkinson, J. H.: 1976, *Phil. Trans. Roy. Soc. London* **A281**, 375.
Švestka, Z.: 1976, *Solar Flares*, D. Reidel Publ. Co., Dordrecht, Holland.
Walker, A. B. C., Jr.: 1972, *Space Sci. Rev.* **13**, 672.
Walker, A. B. C., Jr. and Rugge, H. R.: 1970, *Astron. Astrophys.* **5**, 4.
Walker, A. B. C., Jr. and Rugge, H. R.: 1971, *Astrophys. J.* **164**, 181.
Wolff, R. S.: 1976, *Space Sci. Instrum.* **2**, 263.